

A scenario for the anisotropy of galactic cosmic rays related to nearby source and local regular magnetic field

Ai-feng Li,^a Qiang Yuan,^{b,c} Wei Liu,^{d,1} and Yi-qing Guo^{d,e,1}

^aCollege of Information Science and Engineering, Shandong Agricultural University, Taian 271018, China

^bKey Laboratory of Dark Matter and Space Astronomy, Purple Mountain Observatory, Chinese Academy of Sciences, Nanjing 210008, China

^cSchool of Astronomy and Space Science, University of Science and Technology of China, Hefei 230026, China

^dKey Laboratory of Particle Astrophysics, Institute of High Energy Physics, Chinese Academy of Sciences, Beijing 100049, China

^eUniversity of Chinese Academy of Sciences, Beijing 100049, China

E-mail: liuwei@ihep.ac.cn, guoyq@ihep.ac.cn

Abstract. In our recent work, we build a propagation scenario to simultaneously explain the spectra and anisotropy of cosmic rays (CRs) by considering spatially dependent propagation (SDP) model and nearby Geminga supernova remnant (SNR) source. But the phase of anisotropy is still inconsistent with the experimental data. Recent observations of CR anisotropy show that the phase is consistent with local regular magnetic field (LRMF) observed by Interstellar Boundary Explorer (IBEX) below 100 TeV, which indicates that diffusion along LRMF is important. In this work, we further introduce the LRMF and take into account the effect of corresponding anisotropic diffusion to explain the anisotropy of CRs. We find that when the diffusion coefficient perpendicular to the LRMF is much smaller than the parallel one, the phase of anisotropy points to $\sim R.A. = 3^h$, which accords with experimental observation below 100 TeV. We also analyze the influence of the ratio of perpendicular and parallel diffusion coefficient on the anisotropy and the energy dependence of the ratio. The results illustrate that with the decrease of perpendicular diffusion, the anisotropic phase changes from the direction of nearby source to the LRMF below 100 TeV, meanwhile it changes from the galactic center (GC) to opposite direction of LRMF above 100 TeV. When the perpendicular diffusion coefficient grows faster than the parallel one with energy, the diffusion approaches to the isotropic at high energy, the phase of anisotropy shifts from the LRMF to the GC above 100 TeV. This could be helpful to ascertain the energy dependence of diffusion coefficients.

¹Corresponding author.

²Corresponding author.

Contents

| | | |
|----------|-------------------------------|----------|
| 1 | Introduction | 1 |
| 2 | Model | 2 |
| 2.1 | Spatially dependent diffusion | 2 |
| 2.2 | Local source | 3 |
| 2.3 | Anisotropic diffusion | 3 |
| 2.4 | Large-scale dipole anisotropy | 4 |
| 3 | Results and Discussion | 5 |
| 4 | Summary | 9 |

1 Introduction

Owing to the deflection of the Galactic magnetic field (GMF), CRs lose their original direction and become nearly isotropic. However, small CR anisotropy with relative amplitudes at the order of $10^{-4} \sim 10^{-3}$ is still observed at a wide energy range from 100 GeV to hundreds of TeV. Numerous experiments such as Tibet AS γ [1–3], Super-Kamiokande [4], Milagro [5, 6], IceCube/Ice-Top [7–11], ARGO-YBJ [12, 13], HAWC [14] provided the high-precision and two dimensional observations of CR anisotropy, which show a complex relationship with energy. Less than 100 TeV, the amplitude increases first and then decreases, but increases again above 100 TeV. At the same time the phase reverses from $\sim R.A. = 3^h$ to the GC at an energy of $100 \sim 300$ TeV. The CR anisotropy may arise due to several causes. It may result from the uneven distribution of CR sources such as SNRs [15, 16] or be due to the LRMF which governs the propagation of CRs nearby the solar system [17–19]. The anisotropy can also be a pure kinetic effect called the Compton-Getting effect arising from the relative motion between the observer and the CR plasma [20, 21].

Conventional CR propagation model has been successfully explained many observed phenomena, such as broken power-law energy spectra, secondary-to-primary ratios, the diffuse gamma-ray distribution, etc. However it fails to explain the anisotropy of CRs [22, 23]. It is expected that the amplitude of anisotropy is proportional to the diffusion coefficient $D(\mathcal{R}) \propto \mathcal{R}^\delta$, with $\delta \sim 0.3 - 0.6$. Thus, one can expect that the anisotropy amplitude will increase with energy. But the expected anisotropy amplitude is larger than the observation above hundreds of TeV [22]. Furthermore, conventional CR propagation model expects the anisotropic phase point to GC, because SNRs are mostly in the inner galactic disk region. Nevertheless, the observed phase of anisotropy varies with the energy, especially the phase below 100 TeV is obviously deviated from the GC.

Based on the conventional propagation model, various improvements have been explored to explain the anisotropy problem, including nearby source [15, 16, 23, 24], spatially dependent diffusion process [25–27], ensemble fluctuations of CR sources, etc. Our recent work attempted to explain anisotropy of CRs by involve the nearby source under SDP model [28, 29]. We found that the anisotropic phase of CRs is sensitive to the direction of the nearby source. Because Geminga SNR is located close to the direction of anti GC and far from the galactic disk and it may suppress the expected large amplitude, so it is a prime candidate [30]. Involve

the nearby Geminga SNR source can explain the spectra and amplitude of anisotropy very well, however it couldn't account for the phase of anisotropy which is inconsistent with the observation below 100 TeV [28].

In galaxy, there is GMF with the order of $\sim 3\mu G$, that have two components including regular and the turbulent part. A PeV CR particle with a nucleon number of Z move in a circular motion in GMF with a Larmor radius $r_L \simeq 0.4E_{PeV}/(ZB_{3\mu G})$ pc [19, 31, 32]. The Larmor radius of PeV CRs is much smaller than their scattering length. The propagation of CRs is anisotropic when the regular magnetic field strength is comparable to or beyond that of the turbulent one. Therefore, the anisotropy may be induced by LRMF nearby solar system below PeV [33]. Recently Interstellar Boundary Explorer (IBEX) performed observations of neutral particles which unveiled LRMF [34]. The LRMF is along $(l, b) = (210.5^\circ, -57.1^\circ)$ with an uncertainty of $\sim 1.5^\circ$ within 20 pc. The observation of anisotropic phase of CRs is coincident with the direction of LRMF below 100 TeV. Several literatures [17–19, 35] studied the relationship between anisotropy and LRMF.

The deflecting effect of the magnetic field on the CR particles combined with nearby sources may explain the amplitude and phase of the anisotropy. To demonstrate this view, we introduce LRMF and its corresponding anisotropic diffusion simultaneously considering the contribution of nearby Geminga SNR source under SDP model to account for anisotropy of CRs. In this work, we first calculate the proton, helium and all-particle energy spectra to match the experimental data. Then we analyze the anisotropy of CRs and compare the results with recent work [28]. We find that when the diffusion coefficient perpendicular to the LRMF is much smaller than the parallel one, the phase of anisotropy clearly points to LRMF, which is consistent with the experimental data. We also investigate the influence of the ratio of perpendicular and parallel diffusion coefficient on the anisotropy and the energy dependence of the ratio. This could be helpful to ascertain the ratio and energy dependence of diffusion coefficients.

2 Model

2.1 Spatially dependent diffusion

The region where CRs diffuse in the Milky Way is called a magnetic halo, which is usually approximated as a cylinder with its radial boundary equal to the Galactic radius, i.e. $R = 20$ kpc and its half thickness z_h is about a few kpc. z_h is usually determined by fitting the B/C ratio along with diffusion coefficient [36]. Both CR sources and the interstellar medium are usually assumed to be concentrated near the Galactic disk, whose average thickness z_s is roughly 200 pc.

HAWC observations have recently that the diffusion coefficient of CRs near the galactic disk is at least two orders of magnitude smaller than the conventional one [30]. Therefore, we work in aSDP frame [26, 27, 37], whose diffusion coefficient are different in inner halo and outer halo. The parameterized diffusion coefficient we adopt is [38, 39].

$$D_{xx}(r, z, R) = D_0 F(r, z) \left(\frac{\mathcal{R}}{\mathcal{R}_0}\right)^{\delta_0 F(r, z)} \quad (2.1)$$

| D_0 | δ_0 | N_m | ξ | n | v_A | z_h |
|---------------------------------------|------------|-------|-------|-----|-------------------------------------|-------|
| [$\text{cm}^2 \cdot \text{s}^{-1}$] | | | | | [$\text{km} \cdot \text{s}^{-1}$] | [kpc] |
| 4.87×10^{28} | 0.58 | 0.62 | 0.1 | 4 | 6 | 5 |

Table 1: parameters of SDP model.

$F(r, z)$ is parameterized as

$$F(r, z) = \begin{cases} g(r, z) + [1 - g(r, z)] \left(\frac{z}{\xi z_0}\right)^n, & |z| \leq \xi z_0 \\ 1, & |z| > \xi z_0 \end{cases} \quad (2.2)$$

where $g(r, z) = N_m/[1 + f(r, z)]$, and $f(r, z)$ is the source density distribution. The spatial distribution of sources takes the form of SNR distribution [40]. $f(r, z) \propto (r/r_\odot)^{1.69} \exp[-3.33(r - r_\odot)/r_\odot] \exp(-|z|/z_s)$, where $r_\odot = 8.5$ kpc and $z_s = 0.2$ kpc. In this work, we adopt numerical package DRAGON to solve the transport equation [41]. The corresponding transport parameters are shown in Table 1.

The injection spectrum of background sources is assumed to be a power-law of rigidity with a high-energy exponential cutoff, $q(\mathcal{R}) \propto \mathcal{R}^{-\nu} \exp(-\mathcal{R}/\mathcal{R}_c)$. The cutoff rigidity of each element could be either Z - or A -dependent.

2.2 Local source

Green's function method is adopted to calculate the propagation of particles from the local source, assuming a spherical geometry with infinite boundary conditions [22, 24]. The CR density of local source as a function of space, rigidity, and time is described as

$$\phi(r, \mathcal{R}, t) = \frac{q_{\text{inj}}(\mathcal{R})}{(\sqrt{2\pi}\sigma)^3} \exp\left(-\frac{r^2}{2\sigma^2}\right), \quad (2.3)$$

where $q_{\text{inj}}(\mathcal{R})\delta(t)\delta(\mathbf{r})$ is the instantaneous injection spectrum of a point source, $\sigma(\mathcal{R}, t) = \sqrt{2D(\mathcal{R})t}$ is the effective diffusion length within time t , $D(\mathcal{R})$ is the diffusion coefficient which was adopted as the value nearby the solar system. The injection spectrum is also parameterized as a cutoff power-law form, $q_{\text{inj}}(\mathcal{R}) = q_0 \mathcal{R}^{-\alpha} \exp(-\mathcal{R}/\mathcal{R}'_c)$. The normalization q_0 is obtained through fitting to the CR energy spectra. In this work, we selected the Geminga SNR source ($l, b = 194.3^\circ, -13^\circ$), whose distance and age are $d = 330$ pc and $\tau = 3.4 \times 10^5$ years respectively [30, 42]. The corresponding injection parameters are given in table 2.

2.3 Anisotropic diffusion

Under the anisotropic diffusion model, diffusion of CRs consists of two components: parallel and perpendicular to the magnetic field. The diffusion tensor D_{ij} associated with the magnetic field is written as

$$D_{ij} \equiv D_\perp \delta_{ij} + (D_\parallel - D_\perp) b_i b_j, \quad b_i = \frac{B_i}{|\mathbf{B}|} \quad (2.4)$$

Where b_i is the i -th component of the unit vector [43]. Here D_\parallel and D_\perp are the diffusion coefficients aligned parallel and perpendicular to the regular magnetic field, respectively.

| Element | Background | | | Local source | | |
|---------|---|-------|-----------------|-----------------------|----------|------------------|
| | Normalization [†] | ν | \mathcal{R}_c | q_0 | α | \mathcal{R}'_c |
| | $[(\text{m}^2 \cdot \text{sr} \cdot \text{s} \cdot \text{GeV})^{-1}]$ | | [PV] | $[\text{GeV}^{-1}]$ | | [TV] |
| p | 1.91×10^{-2} | 2.34 | 7 | 8.28×10^{52} | 2.16 | 25 |
| He | 1.43×10^{-3} | 2.27 | 7 | 2.35×10^{52} | 2.08 | 25 |
| C | 6.15×10^{-5} | 2.31 | 7 | 7.2×10^{50} | 2.13 | 25 |
| N | 7.67×10^{-6} | 2.34 | 7 | 1.13×10^{50} | 2.13 | 25 |
| O | 8.20×10^{-5} | 2.36 | 7 | 1.11×10^{51} | 2.13 | 25 |
| Ne | 8.05×10^{-6} | 2.28 | 7 | 1.13×10^{50} | 2.13 | 25 |
| Mg | 1.62×10^{-5} | 2.39 | 7 | 1.08×10^{50} | 2.13 | 25 |
| Si | 1.28×10^{-5} | 2.37 | 7 | 1.05×10^{50} | 2.13 | 25 |
| Fe | 1.23×10^{-5} | 2.29 | 7 | 2.20×10^{50} | 2.13 | 25 |

[†]The normalization is set at total energy $E = 100$ GeV.

Table 2: Injection parameters of the background and local source.

CR particles propagate in a magnetic field, $B = \delta B + B_0$, that is the sum of a regular B_0 field and a turbulent δB field. Mean free path of the CR particles in the TeV region is ~ 20 pc which is larger than the Lamore radius. According to the quasi-linear theory [44, 45], $\delta B(k)^2 = \int d^3 \delta B(k)^2 \ll |B_0|^2$ at this scale. The ratio between the perpendicular and parallel diffusion coefficients is expected to be as

$$\frac{D_{\perp}}{D_{\parallel}} \sim \mathcal{F}(k) \sim \frac{\delta B(k)^2}{B_0^2} \ll 1, \quad (2.5)$$

where $\mathcal{F}(k)$ is the normalized power of the turbulent modes with wave number k [18, 46, 47]. However, if $\delta B/B_0 \sim 1$, $D_{\perp} \simeq D_{\parallel}$, then the diffusion of CRs for higher energies is isotropic. This ratio need to be calculated with the numerical simulation.

In this work, we adopt two different rigidity dependents D_{\parallel} and D_{\perp} following [46],

$$D_{\parallel} = D_{0\parallel} \left(\frac{\mathcal{R}}{\mathcal{R}_0} \right)^{\delta_{\parallel}}, \quad (2.6)$$

$$D_{\perp} = D_{0\perp} \left(\frac{\mathcal{R}}{\mathcal{R}_0} \right)^{\delta_{\perp}} = \varepsilon D_{0\parallel} \left(\frac{\mathcal{R}}{\mathcal{R}_0} \right)^{\delta_{\perp}}, \quad (2.7)$$

which $\varepsilon = \frac{D_{0\perp}}{D_{0\parallel}}$ is the ratio between perpendicular and parallel diffusion coefficient at the reference rigidity \mathcal{R}_0 . The parameters δ_{\parallel} , δ_{\perp} , \mathcal{R}_0 , and ε need to be carefully chosen to keep $D_{\perp} \lesssim D_{\parallel}$ within the concerned energy region(GeV - PeV).

2.4 Large-scale dipole anisotropy

In a simple model of isotropic diffusion, the amplitude of the dipole anisotropy is usually defined with observed relative difference between the fluxes in the maximum and minimum

directions ϕ_{\max} and ϕ_{\min} as [18]

$$|\delta| = \frac{(\phi_{\max} - \phi_{\min})}{(\phi_{\max} + \phi_{\min})} = \frac{3D \cdot \nabla\psi}{v\psi}, \quad (2.8)$$

It can be seen that the amplitude of the dipole anisotropy is proportional to the spatial gradient of the CR density $\nabla\psi$ and the diffusion coefficient D .

In anisotropic diffusion model, its vector form can be written as [19, 35]

$$\delta = \frac{3}{v\psi} D_{ij} \frac{\partial\psi}{\partial x_j}. \quad (2.9)$$

The rigidity dependence of the dipole amplitude results from both diffusion tensor D_{ij} and $\frac{\nabla\psi}{\psi}$. For GeV–PeV CRs, parallel diffusion predominates, the anisotropic phase tends to the direction of magnetic field. In order to study the influence of two diffusion coefficients (D_{\perp} and D_{\parallel}) on anisotropy, we would choose several sets of parameters (ε , δ_{\parallel} , δ_{\perp}) to calculate the anisotropy.

3 Results and Discussion

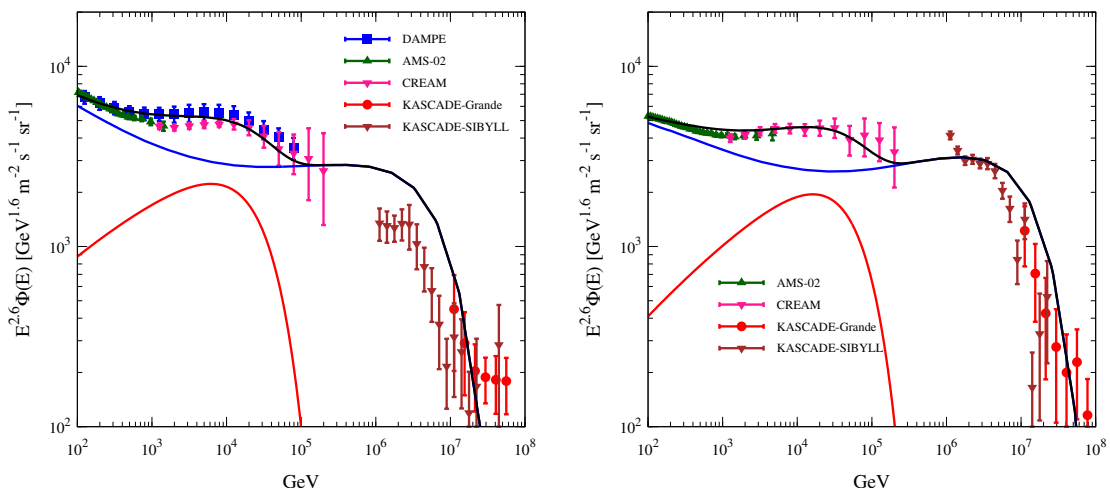


Figure 1: Energy spectra of protons (left) and helium nuclei (right). The data points are taken from DAMPE[48, 49], AMS-02 [50, 51], CREAM-III [52], NUCLEON [53], KASCADE [54] and KASCADE-Grande [55] respectively. The blue lines are the background fluxes, and the red lines are the fluxes from a nearby Geminga SNR source respectively. The black lines represent the sum contributions of the background and nearby Geminga SNR source.

The LRMF within 20 pc has been measured accurately by IBEX experiment, which is much smaller than the size of the Milky Way [34, 46]. Therefore, when we simulate the CRs background using DRAGON public numerical packages [41], the CRs is approximately isotropic diffusion in the Milky Way. First, we calculate the proton and helium spectra. Figure 1 shows the energy spectra of protons and helium obtained for the model calculation, with the red, blue and black lines representing the contributions from the local source, the

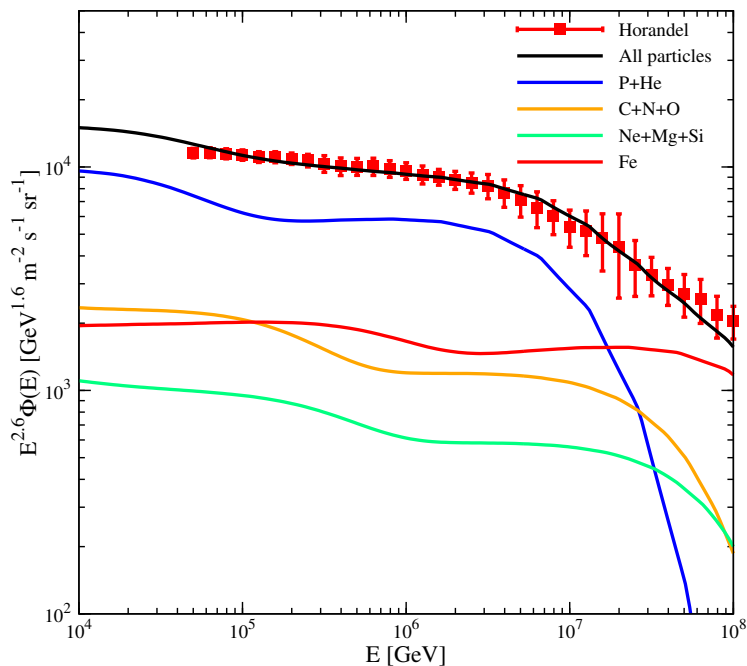


Figure 2: The all-particle spectra multiplied by $E^{2.6}$. The data points are taken from ref [56]. The solid lines with different colors are the model predictions of different mass groups, and the black solid line is the total contribution.

background sources and the sum of them, respectively. It can be seen that the contribution of nearby Geminga SNR source can simultaneously account for the spectral hardening features at ~ 200 GeV, and softening features at ~ 10 TeV. Through adding different compositions together, we get the all-particle spectrum as shown in Figure 2, which is well consistent with the observational data.

The anisotropy of CRs depends on the sum of the CR flows from the background and the local source. In this work, the parameters of parallel diffusion coefficient D_{\parallel} are set as those shown in Table 1. The CRs in the 100 GeV - PeV energy region require $D_{\parallel} > D_{\perp}$, therefore we set $\varepsilon = 0.01$ and $\Delta\delta = \delta_{\perp} - \delta_{\parallel} = 0.32$, where $\Delta\delta$ is the difference between δ_{\perp} and δ_{\parallel} . Figure 3 shows the comparison of the anisotropy of CRs with and without LRMF [28], where the solid black line presents anisotropy of the introduced LRMF and its anisotropic diffusion effect combined with nearby Geminga SNR source, and red broken line is the result of the work [28], respectively. For $E < 100$ TeV, anisotropic phase with the LRMF clearly points to LRMF ($\sim R.A. = 3^h$), which is better in accordance with the experimental observation than the result without magnetic field. The nearby source dominates the observed anisotropies, although its flux is sub-dominant. The position of nearby source and the direction of LRMF together determine the anisotropic phase. The phase flips at 100 TeV from $\sim R.A. = 3^h$ to GC. For $E \gtrsim 100$ TeV, the contribution from the local source and LRMF decrease significantly, and background become dominant instead. The phase of the anisotropy turns to the GC, since CR sources are more abundant in the inner Galaxy.

Anisotropy of CRs is related to the diffusion coefficient, which is determined by the parameters ε , δ_{\parallel} , δ_{\perp} , and \mathcal{R}_0 . To study the induced anisotropy changes of CRs by the ratio

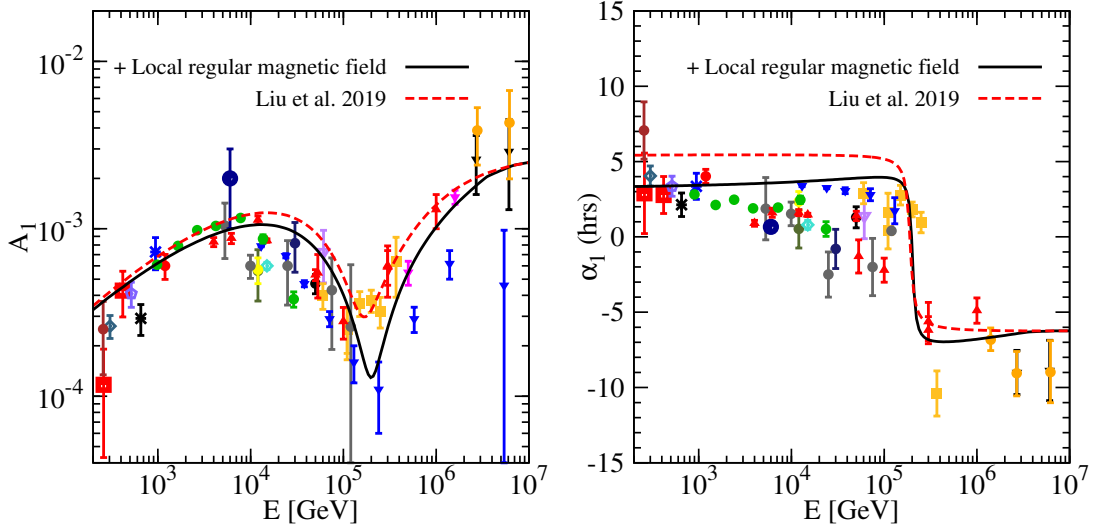


Figure 3: When $\varepsilon = 0.01$, $\Delta\delta = 0.32$, energy dependences of the amplitude (left) and phase (right) of the dipole anisotropies together with the contribution from nearby Geminga SNR source and LRMF. The red broken line indicates the result [28].

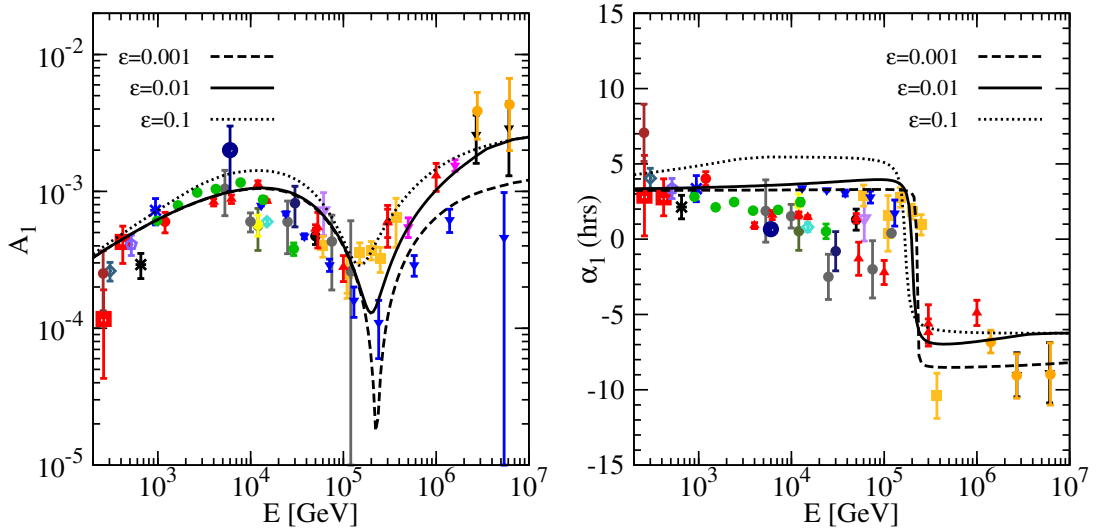


Figure 4: Energy dependences of the amplitude (left) and phase (right) of the anisotropies for $\Delta\delta(\delta_{\perp} - \delta_{\parallel}) = 0.32$ together with the contribution from nearby Geminga SNR source and local regular magnetic field. The three black lines correspond to the results for three different $\varepsilon(= 0.1, 0.01, 0.001)$.

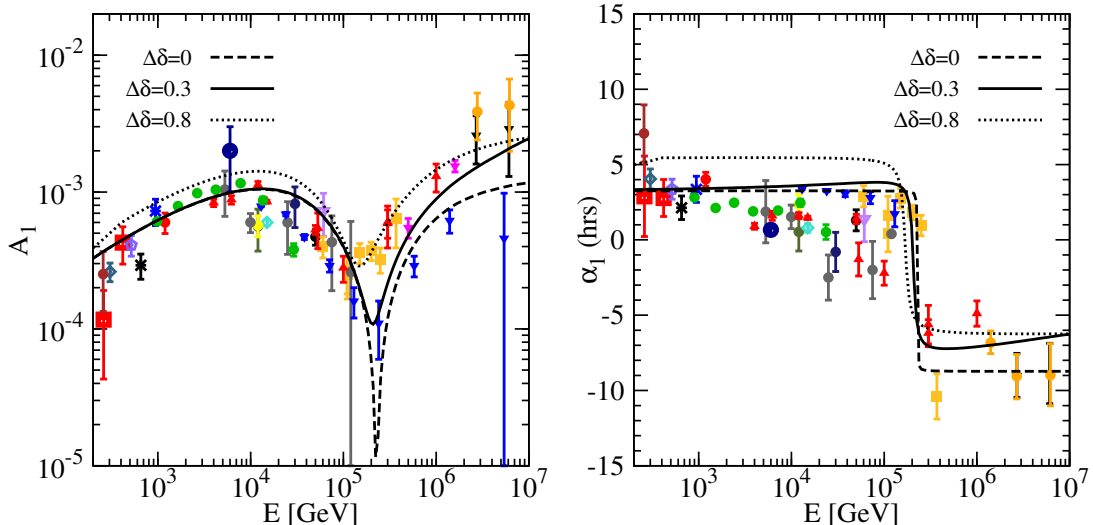


Figure 5: Energy dependences of the amplitude (left) and phase (right) of the anisotropies for $\varepsilon = 0.01$ together with the contribution from nearby Geminga SNR source and LRMF. The three black lines correspond to the results for three different $\Delta\delta(\delta_{\perp} - \delta_{\parallel})(= 0, 0.3, 0.8)$.

of perpendicular and parallel diffusion coefficients, we calculate the anisotropy of different ε (0.1, 0.01, 0.001) at $\Delta\delta = 0.32$. Figure 4 shows the anisotropies of three different ε and demonstrates the amplitude and phase of anisotropy are significantly related to ε . At the same energy, the amplitude of anisotropy increases with increasing of ε , which is due to the amplitude is proportional to the diffusion coefficient. As ε decreases from 0.1 to 0.001, the phase of anisotropy shifts from the position of the nearby source to the LRMF below 100 TeV, that results from the parallel diffusion gradually increases and the perpendicular diffusion weakens. At the same time, the phase of anisotropy shifts from the GC to opposite direction of LRMF above 100 TeV.

In addition to ε , we also study the relationship between anisotropy and $\Delta\delta$. Figure 5 shows the amplitude and phase of the anisotropy with different $\Delta\delta$ (0, 0.3 and 0.8) at $\varepsilon=0.01$. From Figure 5 (left), we can see that with the increase of $\Delta\delta$, the anisotropic amplitude of CRs rises, which is due to the diffusion coefficient become larger. Figure 5 (right) illustrates that with the increase of $\Delta\delta$, anisotropic phase of CRs changes from the LRMF to the direction of the nearby source below 100 TeV, while it changes from the opposite direction of LRMF to GC above 100 TeV. It can be attributed to that the diffusion gradually transforms from anisotropic to the isotropic, when perpendicular diffusion coefficient grows faster than the parallel one. The current experimental observation around PeV energy range are still in dispute. The AS γ measurement points to the GC, while the ICECUBE observation points to the LRMF. Further experimental measurements of anisotropic phase, such as LHAASO, will help to understand the energy dependence of the diffusion coefficient.

4 Summary

The observation of CR anisotropy is hard to explain for a long time. Our recent work attempted to account for the anisotropy of CRs through the contribution of nearby Geminga SNR source under the SDP model. However the anisotropic phase is about $\sim R.A. = 5^h$ below 100 TeV, which disagrees with the experimental data. LRMF observed by IBEX is coincident with observational phase of anisotropy, which indicates that diffusion along LRMF is important. Here, we further take into account the LRMF and the corresponding effect of anisotropic diffusion on CR anisotropy.

We find that when the diffusion coefficient perpendicular to the LRMF is much smaller than the parallel one, i.e. the CR propagation is principally along the magnetic field, the phase of anisotropy changes from the direction of local source to the LRMF, which conforms with the observations below 100 TeV.

We further study the influence of the ratio of the perpendicular and parallel diffusion coefficients on anisotropy. When the perpendicular diffusion coefficient becomes smaller, the phase of anisotropy gradually shifts from the local source to the LRMF below 100 TeV, while it shifts from the GC to the opposite direction of LRMF above 100 TeV.

We also investigate the energy dependence of the ratio. When the perpendicular diffusion coefficient grows faster than the parallel one with energy, the diffusion approaches to the isotropic at high energy, the phase of anisotropy changes from the LRMF to the GC above 100 TeV. However the current measurements at that energy range are still in dispute. The Tibet AS γ measurement points to the GC, while the ICECUBE observation points to the LRMF. We hope that the CR experiments, for example LHAASO, could measure the anisotropy phase precisely, which could be helpful to ascertain the energy dependence of diffusion coefficients.

Overall, we provide a good scenario for anisotropy of CRs related to nearby Geminga SNR source and LRMF inferred from IBEX, in the energy region from 100 GeV to PeV.

Acknowledgements

This work is supported by the National Key *R&D* Program of China grant (2018YFA0404202) and the National Natural Science Foundation of China (11963004, 11635011, 11875264, U1831208, U1738205, U2031110) and Shandong Province Natural Science Foundation (ZR2020MA095).

References

- [1] M. Amenomori, S. Ayabe, X. J. Bi, et al. Anisotropy and Corotation of Galactic Cosmic Rays. *Science*, 314(5798):439–443, October 2006.
- [2] M. Amenomori et al. On Temporal Variations of the Multi-TeV Cosmic Ray Anisotropy using the Tibet III Air Shower Array. *Astrophys. J.*, 711:119–124, 2010.
- [3] M. Amenomori. Northern sky Galactic Cosmic Ray anisotropy between 10-1000 TeV with the Tibet Air Shower Array. *Astrophys. J.*, 836(2):153, 2017.
- [4] G. Guillian, J. Hosaka, K. Ishihara, et al. Observation of the anisotropy of 10TeV primary cosmic ray nuclei flux with the Super-Kamiokande-I detector. *Phys. Rev. D*, 75(6):062003, March 2007.
- [5] A. A. Abdo, B. Allen, T. Aune, et al. Discovery of Localized Regions of Excess 10-TeV Cosmic Rays. *Physical Review Letters*, 101(22):221101, November 2008.

- [6] A. A. Abdo, B. T. Allen, T. Aune, et al. The Large-Scale Cosmic-Ray Anisotropy as Observed with Milagro. *apj*, 698:2121–2130, June 2009.
- [7] R. Abbasi, Y. Abdou, T. Abu-Zayyad, et al. Measurement of the Anisotropy of Cosmic-ray Arrival Directions with IceCube. *apj*, 718:L194–L198, August 2010.
- [8] R. Abbasi, Y. Abdou, T. Abu-Zayyad, et al. Observation of Anisotropy in the Arrival Directions of Galactic Cosmic Rays at Multiple Angular Scales with IceCube. *apj*, 740:16, October 2011.
- [9] R. Abbasi, Y. Abdou, T. Abu-Zayyad, et al. Observation of Anisotropy in the Galactic Cosmic-Ray Arrival Directions at 400 TeV with IceCube. *apj*, 746:33, February 2012.
- [10] M. G. Aartsen, R. Abbasi, Y. Abdou, et al. Observation of Cosmic-Ray Anisotropy with the IceTop Air Shower Array. *apj*, 765:55, March 2013.
- [11] M. G. Aartsen, K. Abraham, M. Ackermann, et al. Anisotropy in Cosmic-Ray Arrival Directions in the Southern Hemisphere Based on Six Years of Data from the IceCube Detector. *apj*, 826:220, August 2016.
- [12] B. Bartoli, P. Bernardini, X. J. Bi, et al. Medium scale anisotropy in the TeV cosmic ray flux observed by ARGO-YBJ. *prd*, 88(8):082001, October 2013.
- [13] B. Bartoli, P. Bernardini, X. J. Bi, et al. ARGO-YBJ Observation of the Large-scale Cosmic Ray Anisotropy During the Solar Minimum between Cycles 23 and 24. *apj*, 809:90, August 2015.
- [14] A. U. Abeysekara, R. Alfaro, C. Alvarez, et al. Observation of Small-scale Anisotropy in the Arrival Direction Distribution of TeV Cosmic Rays with HAWC. *apj*, 796:108, December 2014.
- [15] A. D. Erlykin and A. W. Wolfendale. The anisotropy of galactic cosmic rays as a product of stochastic supernova explosions. *Astroparticle Physics*, 25:183–194, April 2006.
- [16] P. Blasi and E. Amato. Diffusive propagation of cosmic rays from supernova remnants in the Galaxy. I: spectrum and chemical composition. *jcap*, 1:10, January 2012.
- [17] N. A. Schwadron, F. C. Adams, E. R. Christian, et al. Global Anisotropies in TeV Cosmic Rays Related to the Sun rsquo s Local Galactic Environment from IBEX. *Science*, 343:988–990, February 2014.
- [18] P. Mertsch and S. Funk. Solution to the Cosmic Ray Anisotropy Problem. *Physical Review Letters*, 114(2):021101, January 2015.
- [19] M. Ahlers. Deciphering the Dipole Anisotropy of Galactic Cosmic Rays. *Physical Review Letters*, 117(15):151103, October 2016.
- [20] Arthur H. Compton and Ivan A. Getting. An Apparent Effect of Galactic Rotation on the Intensity of Cosmic Rays. *Physical Review*, 47(11):817–821, June 1935.
- [21] L. J. Gleeson and W. I. Axford. The Compton-Getting Effect. *Ap&SS*, 2(4):431–437, December 1968.
- [22] P. Blasi and E. Amato. Diffusive propagation of cosmic rays from supernova remnants in the Galaxy. II: anisotropy. *jcap*, 1:11, January 2012.
- [23] Wei Liu, Xiao-Jun Bi, Su-Jie Lin, Bing-Bing Wang, and Peng-Fei Yin. Excesses of cosmic ray spectra from a single nearby source. *prd*, 96(2):023006, July 2017.
- [24] L. G. Sveshnikova, O. N. Strelnikova, and V. S. Ptuskin. Spectrum and anisotropy of cosmic rays at TeV-PeV-energies and contribution of nearby sources. *Astroparticle Physics*, 50:33–46, December 2013.
- [25] C. Evoli, D. Gaggero, D. Grasso, and L. Maccione. Common Solution to the Cosmic Ray Anisotropy and Gradient Problems. *Physical Review Letters*, 108(21):211102, May 2012.

- [26] N. Tomassetti. Origin of the Cosmic-Ray Spectral Hardening. *apj*, 752:L13, June 2012.
- [27] Y.-Q. Guo, Z. Tian, and C. Jin. Spatial-dependent Propagation of Cosmic Rays Results in the Spectrum of Proton, Ratios of P/P, and B/C, and Anisotropy of Nuclei. *ApJ*, 819:54, March 2016.
- [28] Wei Liu, Yi-Qing Guo, and Qiang Yuan. Indication of nearby source signatures of cosmic rays from energy spectra and anisotropies. *jcap*, 2019(10):010, October 2019.
- [29] Bing-Qiang Qiao, Wei Liu, Yi-Qing Guo, and Qiang Yuan. Anisotropies of different mass compositions of cosmic rays. *jcap*, 2019(12):007, December 2019.
- [30] A. U. Abeysekara, A. Albert, R. Alfaro, et al. Extended gamma-ray sources around pulsars constrain the origin of the positron flux at Earth. *Science*, 358(6365):911–914, November 2017.
- [31] Markus Ahlers and Philipp Mertsch. Origin of small-scale anisotropies in Galactic cosmic rays. *Progress in Particle and Nuclear Physics*, 94:184–216, May 2017.
- [32] A. P. Snodin, A. Shukurov, G. R. Sarson, P. J. Bushby, and L. F. S. Rodrigues. Global diffusion of cosmic rays in random magnetic fields. *MNRAS*, 457(4):3975–3987, April 2016.
- [33] Eduardo Battaner, Joaquín Castellano, and Manuel Masip. Galactic Magnetic Fields and the Large-Scale Anisotropy at Milagro. *ApJ*, 703(1):L90–L93, September 2009.
- [34] H. O. Funsten, R. DeMajistre, P. C. Frisch, et al. Circularity of the Interstellar Boundary Explorer Ribbon of Enhanced Energetic Neutral Atom (ENA) Flux. *ApJ*, 776(1):30, Oct 2013.
- [35] Wei Liu, Su-jie Lin, Hong-bo Hu, Yi-qing Guo, and Ai-feng Li. Two Numerical Methods for the 3D Anisotropic Propagation of Galactic Cosmic Rays. *ApJ*, 892(1):6, March 2020.
- [36] Andrew W. Strong, Igor V. Moskalenko, and Vladimir S. Ptuskin. Cosmic-Ray Propagation and Interactions in the Galaxy. *Annual Review of Nuclear and Particle Science*, 57(1):285–327, November 2007.
- [37] Chao Jin, Yi-Qing Guo, and Hong-Bo Hu. Spatial dependent diffusion of cosmic rays and the excess of primary electrons derived from high precision measurements by AMS-02. *Chinese Physics C*, 40(1):015101, January 2016.
- [38] Yi-Qing Guo and Qiang Yuan. Understanding the spectral hardenings and radial distribution of Galactic cosmic rays and Fermi diffuse γ rays with spatially-dependent propagation. *Phys. Rev. D*, 97(6):063008, March 2018.
- [39] Wei Liu, Yu-hua Yao, and Yi-Qing Guo. Revisiting the Spatially Dependent Propagation Model with the Latest Observations of Cosmic-Ray Nuclei. *ApJ*, 869(2):176, December 2018.
- [40] G. Case and D. Bhattacharya. Revisiting the galactic supernova remnant distribution. *A&AS*, 120:437–440, December 1996.
- [41] Carmelo Evoli, Daniele Gaggero, Dario Grasso, and Luca Maccione. Cosmic Ray propagation in the Galaxy and diffuse gamma-ray emission. In Felix A. Aharonian, Werner Hofmann, and Frank Rieger, editors, *American Institute of Physics Conference Series*, volume 1085 of *American Institute of Physics Conference Series*, pages 380–383, December 2008.
- [42] Jacqueline Faherty, Frederick M. Walter, and Jay Anderson. The trigonometric parallax of the neutron star Geminga. *Ap&SS*, 308(1-4):225–230, April 2007.
- [43] J. Giacalone and J. R. Jokipii. The Transport of Cosmic Rays across a Turbulent Magnetic Field. *ApJ*, 520:204–214, July 1999.
- [44] J. R. Jokipii. Cosmic-Ray Propagation. I. Charged Particles in a Random Magnetic Field. *ApJ*, 146:480, November 1966.
- [45] J. R. Jokipii and E. N. Parker. Random Walk of Magnetic Lines of Force in Astrophysics. *Phys. Rev. Lett.*, 21(1):44–47, July 1968.

- [46] S. S. Cerri, D. Gaggero, A. Vittino, C. Evoli, and D. Grasso. A signature of anisotropic cosmic-ray transport in the gamma-ray sky. *jcap*, 10:019, October 2017.
- [47] Eduardo Battaner, Joaquín Castellano, and Manuel Masip. Magnetic Fields and Cosmic-Ray Anisotropies at TeV Energies. *ApJ*, 799(2):157, February 2015.
- [48] Q. An, R. Asfandiyarov, P. Azzarello, et al. Measurement of the cosmic ray proton spectrum from 40 GeV to 100 TeV with the DAMPE satellite. *Science Advances*, 5(9):eaax3793, September 2019.
- [49] F. Alemanno, Q. An, P. Azzarello, et al. Measurement of the Cosmic Ray Helium Energy Spectrum from 70 GeV to 80 TeV with the DAMPE Space Mission. *Phys. Rev. Lett.*, 126(20):201102, May 2021.
- [50] M. Aguilar, D. Aisa, B. Alpat, et al. Precision Measurement of the Proton Flux in Primary Cosmic Rays from Rigidity 1 GV to 1.8 TV with the Alpha Magnetic Spectrometer on the International Space Station. *Phys. Rev. Lett.*, 114(17):171103, May 2015.
- [51] M. Aguilar, L. Ali Cavazonza, B. Alpat, et al. Observation of the Identical Rigidity Dependence of He, C, and O Cosmic Rays at High Rigidities by the Alpha Magnetic Spectrometer on the International Space Station. *Phys. Rev. Lett.*, 119(25):251101, December 2017.
- [52] Y. S. Yoon, T. Anderson, A. Barrau, et al. Proton and Helium Spectra from the CREAM-III Flight. *ApJ*, 839(1):5, April 2017.
- [53] E. Atkin, V. Bulatov, V. Dorokhov, et al. First results of the cosmic ray NUCLEON experiment. *J. Cosmology Astropart. Phys.*, 2017(7):020, July 2017.
- [54] T. Antoni, W. D. Apel, A. F. Badea, et al. KASCADE measurements of energy spectra for elemental groups of cosmic rays: Results and open problems. *Astroparticle Physics*, 24(1-2):1–25, September 2005.
- [55] W. D. Apel, J. C. Arteaga-Velázquez, K. Bekk, et al. KASCADE-Grande measurements of energy spectra for elemental groups of cosmic rays. *Astroparticle Physics*, 47:54–66, July 2013.
- [56] Jörg R. Hörandel. On the knee in the energy spectrum of cosmic rays. *Astroparticle Physics*, 19(2):193–220, May 2003.